UXO CLASSIFICATION USING CHARACTERISTIC MODES OF THE BROADBAND ELECTROMAGNETIC INDUCTION RESPONSE

D.D. Snyder, Scott MacInnes, Scott Urquhart, and K.L. Zonge
Zonge Engineering and Research Organization, Inc.
3322 E. Fort Lowell Rd., Tucson, Arizona USA 85716

Variations of this paper have been presented at the following conferences:

1. A New Technology Applications Conference on the Science and Technology of Unexploded Ordnance (UXO) Removal and site Remediation. Outrigger Wailea Resort, Maui, HI, November 8-11, 1999.
2. SAGEEP 2000, Arlington, VA, February 20-24, 2000 (Proceedings, p. 747)
3. Pacific Environmental Restoration Conference, Honolulu, HI, April 4-7, 2000

UXO CLASSIFICATION USING CHARACTERISTIC MODES OF THE BROADBAND ELECTROMAGNETIC INDUCTION RESPONSE

D.D. Snyder, Scott MacInnes, Scott Urquhart, and K.L. Zonge
Zonge Engineering and Research Organization, Inc.
3322 E. Fort Lowell Rd., Tucson, Arizona USA 85716

ABSTRACT

Electromagnetic induction methods are effective in locating unexploded ordnance (UXO). However, the induction EM instruments that are used for UXO detection generally have limited bandwidths and provide little, if any, information for UXO classification. It is well known that the broadband induction EM response from confined conductors (such as UXO) can be parameterized in the time-domain as a series of damped exponential decay curves, and in the frequency domain as a set of discrete real first order poles and their residues. Characteristic decay time or its equivalent real pole has been shown to be a function of characteristic target dimensions, target conductivity, and relative magnetic permeability. Therefore, parameterization of the broadband EM response in terms of these characteristic modes provides a basis for the classification of UXO anomalies.

In this paper we have used a numerical method (Prony) to analyze TEM decay curves to obtain a set of exponential decay time-constants and their corresponding residues. Using a commercially available field data acquisition system, we have acquired fast transient TEM data from UXO. We show that these data can be analyzed and displayed in a way that is simple to understand and useful for classifying the TEM response.

1.0 INTRODUCTION

The measurement of the broadband induction electromagnetic response in the form of a complex function of frequency (FEM) or, alternatively, as a transient function of time (TEM) has been applied in geophysical exploration for 30 years or more. Until recently, however, broadband induction EM methods have not been routinely applied for shallow exploration problems because the frequency band of interest is too high for common induction EM instruments. Only a few field instruments are available with the requisite bandwidth for effective broadband EM sounding and/or prospecting in the shallow subsurface (< 30 m).

The potential of using the broadband induction EM response as a basis for classifying metallic targets is generally recognized. In the context of UXO, McNeill et. al. [1], concluded that *". . ., given "a priori" knowledge of the decay characteristics of UXO that are expected in a survey area, the evidence presented in this paper suggests that it might be possible to separate out various types of UXO (a) from each other and (b) from exploded ordnance and other trash metal."* Ongoing research and development is directed toward developing instruments and techniques for object detection and classification using broadband induction EM [2]([3] ch 6).

In this paper, we investigate how broadband induction EM responses can provide a basis for UXO classification. We review some important characteristics of the inductive EM response of confined conductors. These characteristics justify decomposing a TEM transient into a series of

characteristic modal functions whose parameters are functions of conductivity and size characteristics of the target. We apply Prony's method to decompose both synthetic and real TEM transients into these characteristic modes.

2.0 THE BROADBAND EM RESPONSE OF CONFINED CONDUCTORS

Baum ([3] ch 6) has developed a unified theory for the induction EM response of small highly conducting and magnetically permeable objects such as UXO. The theory of UXO detection and characterization with induction EM is simplified by making assumptions that, for the most part, are fully justified by the nature of the target. The assumptions are:

1) UXO have electrical conductivity that is at least 6 orders of conductivity higher than its host medium (soil). To a good approximation, therefore, we can assume that the host medium is non-conducting (i.e., σ=0).
2) UXO is generally fabricated from steel with a relative magnetic permeability that runs as high as 200. Typical host soils have low relative permeability (~1). We therefore assume that the permeability of the host medium is μ_0.
3) At the frequencies employed, UXO are electrically small. That is, the characteristic dimensions of the UXO are very much smaller than a free-space wavelength of electromagnetic radiation in the host medium. (Quasi-static approximation)
4) UXO has a fully three-dimensional geometry with characteristic dimensions that are small compared with the distance from the sensor array. We can assume, therefore, that the magnetic field generated by the transmitter is uniform over the target volume and that secondary magnetic fields are approximated by a simple point dipole source with a time or frequency-dependent moment.

The electromagnetic responses of bodies that satisfy assumptions 1-3 have been termed ***confined conductors*** by Kaufman [4]. Kaufman concludes that the spectrum of the magnetic field created by eddy currents in a confined conductor can be represented as the sum of simple poles located along the negative real axis and takes the form:

$$h(t) = \sum_{m=1}^{\infty} B_m e^{s_m t} \tag{1}$$

where $h(t)$ = magnetic field intensity

t = time

$s_m = 1/\tau_m$ the mth pole of the induced magnetic field (all negative real numbers)

B_m = the coefficient for the series expansion (termed the *residue* of the pole)

Values for the poles and residues (i.e., s_m, and B_m) can be determined analytically for only a few geometrical shapes having surfaces that correspond with coordinate surfaces of special orthogonal coordinate systems (e.g., spheres). Kaufman [5] has tabulated formulas for the principal (i.e., longest) time constants of various canonical shapes.

2.1 Conducting Permeable Sphere

The conducting permeable sphere is a simple three-dimensional shape for which an analytic solution for the inductive EM response is available. We use the behavior of the sphere to illustrate the general behavior of the broadband EM response for the more general class of confined conductors. Wait and Spies [6] have developed the theory for the transient response of a conducting permeable sphere in a uniform time varying field. The secondary field of the sphere behaves like a point dipole located at the center of the sphere. The mathematical behavior of the dipole ([3] ch 6) is

$$\vec{H}_s = \frac{1}{4\pi r^5}\left[3(\vec{r}\vec{r}) - r^2\vec{\vec{I}}\right]\cdot\left(\vec{\vec{M}}\cdot\vec{H}_0\right), \tag{2}$$

where (see Figure 1)

$\vec{H}_0, \vec{H}_s$ $\Rightarrow$ the primary and secondary magnetic fields, respectively

$\vec{M} = \vec{\vec{M}}\cdot\vec{H}_0 \Rightarrow$ Induced Magnetic Moment

$\vec{\vec{M}} \Rightarrow$ Magnetic Polarizability

$\vec{\vec{I}}$ $\Rightarrow$ The identity dyadic

$r = |\vec{r}|$ $\Rightarrow$ The position vector directed from the dipole to P.

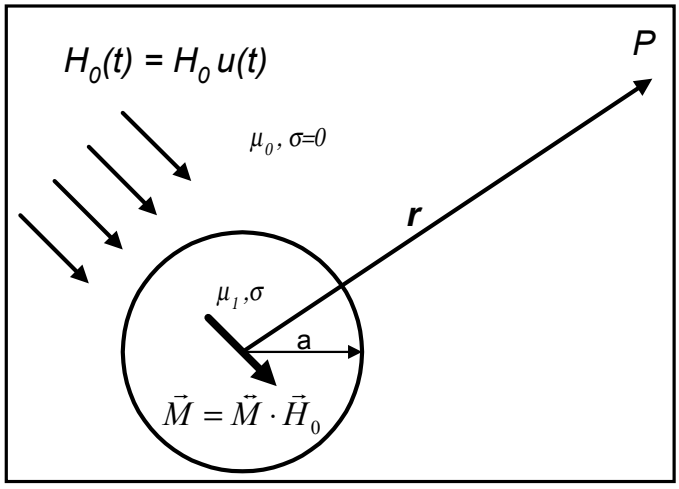

Figure 1: Conducting Permeable Sphere

The behavior of the secondary field (H_s) as a function of frequency or time is entirely contained in the moment term of equation (2). All other terms are purely geometrical. The direction of the moment is controlled by the direction of the primary field (H_0) and the magnetic polarizability dyadic ($\vec{\vec{M}}$). The location of the dipole target in space can be determined by observing the field response at different points in space.

The solution for the transient response of the conducting permeable sphere (see Figure 1) in a uniform non-conducting medium when illuminated by a constant uniform field that starts abruptly at time $t=0$ is [6]

$$h(t) = \left[6K\sum_{n=1}^{\infty}\frac{e^{-\frac{\delta_n^2 T}{K}}}{(K+2)(K-1)+\delta_n^2} - \frac{2(K-1)}{K+2}\right]u(T) \tag{3}$$

where $h(t) = m(t)/2\pi a^3 H_0$ = normalized transient magnetic field moment

K = relative magnetic permeability ($\mu_1 = K\mu_0$)

T = $t/(\mu_0\sigma a^2)$ dimensionless time

δ_n = Solutions to $\tan\delta_n = \dfrac{(K-1)\delta_n}{K-1+\delta_n^2}$ (3a)

$u(t)$ = 0 ($t < 0$)
= 1 ($t > 0$)

Most TEM systems, including the Zonge system used in this paper, measure the impulsive response that is proportional to the negative time derivative of equation (3).

$$-\frac{dh(t)}{dt}=\frac{-1}{\mu_0 a^2\sigma}\frac{dh(t)}{dT}=\frac{1}{\mu_0 a^2\sigma}\left[6\sum_{n=1}^{\infty}\frac{\delta_n^2\, e^{-\frac{\delta_n^2 T}{K}}}{(K+2)(K-1)+\delta_n^2}-\delta(T)\right] \tag{4}$$

The transient behavior of magnetic fields generated by the magnetic dipole moment implied in (3) and (4) is therefore characterized by an infinite series of exponential decay terms. Figure 2 plots transients generated by equation (4) for a range of the relative permeability (K) as a

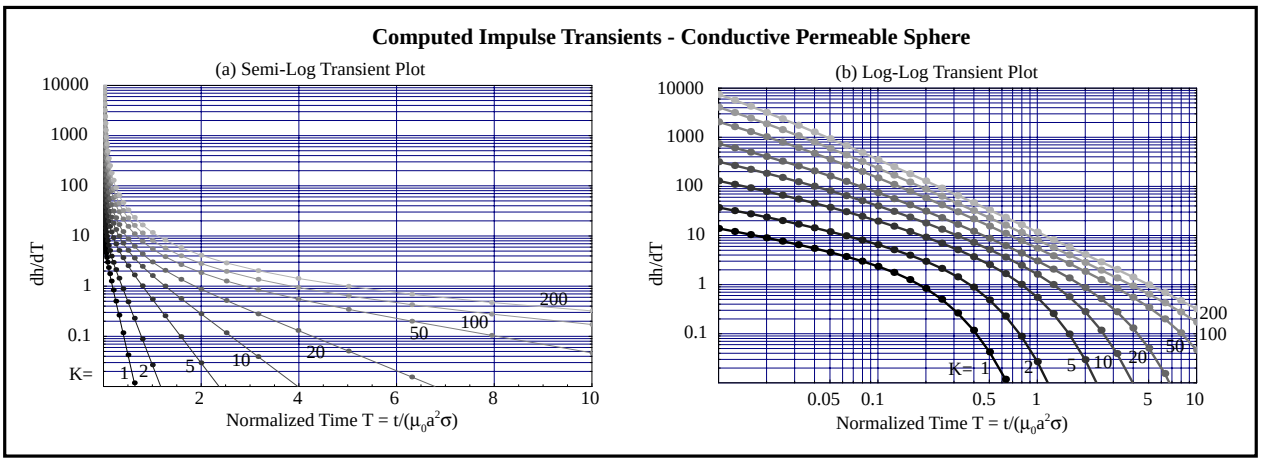

Figure 2: Theoretical decay transients

function of the dimensionless time $T=t/(\sigma\mu_0 a^2)$. (Amplitudes have been normalized by $\mu_0 a^2\sigma$.) TEM decay curves are best displayed in semi-log (Figure 2a) or log-log format (Figure 2b). The exponential behavior of the TEM decay transient for confined conductors is best illustrated in the semi-log plot. The large dynamic range of TEM transients in both time and amplitude makes the log-log plot the best for general display. Note that the transient curve exhibits a near log-log linear behavior (Figure 2b) at high relative permeabilities. This behavior suggests that the high order time constants are sensitive indicators of target permeability.

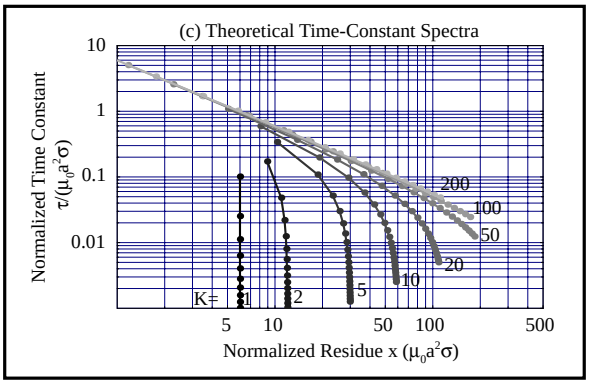

Figure 3: Time-Constant Spectra (Sphere)

The time constants and residues are plotted as time-constant spectra in Figure 3. Normalized time constants ($\tau/\mu_0\sigma a^2 = K/\delta_n^2$) are plotted versus the corresponding residue term, with the relative permeability (K = 1, 2, 5, 20, 50, 100, 200) as the curve parameter. The range of relative permeability ($1 \le K \le 200$) is representative of UXO.[1] The spectra are discrete.

[1] Sower ([3] ch 8) observes that the relative permeability of ferrous objects is a function of the field strength of the polarizing field. While at low field strengths the permeability is 200, that permeability can reach as high as 5000 at higher field strengths. He notes that most commercially available iron and steel saturates at a field strength of about 80 A/m, a value which is easily generated by a multi-turn transmitter loop carrying several amperes of current.

2.2 Analysis by Characteristic Modes

To exploit the basic physics of the broadband EM response of confined conductors, we must determine values for the time constants and their residues. The residues are functions of transmitter and receiver position and of the amplitude of the primary magnetic field (H_0) as indicated in equation (3). Time constants, however, are intrinsic characteristics of the target and are like the ***natural*** or ***characteristic*** frequencies of many dynamical systems.

Techniques for computing the time constants and coefficients have frequently appeared in the literature [7]. We have chosen Prony's method for the analysis of TEM transients. We make no representations as to the efficacy of this method for application to TEM transients. However, the method is used for analysis of radar and sonar transients. We will not describe Prony's method in any detail. Suffice it to say that Prony's algorithm requires a minimum of 2N samples of the decay transient (at uniform time intervals) in order to determine a set of N poles and N residues.

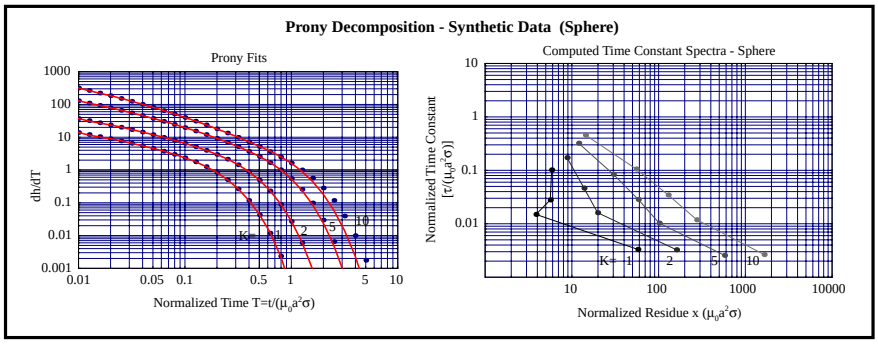

Figure 4: Computed Time-Constant Spectra Conducting

We applied Prony's method to the data sets shown in Figure 2 using a dimensionless sample interval of 0.01. The results (Figure 4-left) are plotted as transient plots showing the observed data (points), and the corresponding curve fit (lines). Figure 4 (right) shows the time-constant spectra corresponding to each of the synthetic transients analyzed. Prony analysis effectively resolves at least three of the poles. Obvious differences in the fit of the curves for K=5 and K=10 are caused by the choice of digitization interval and the total time interval of the computed transients.

3.0 EXPERIMENTAL DATA COLLECTION AND ANALYSIS

In principle, the time-constant spectra provide a basis for the classification of conducting permeable targets such as UXO. As we have seen from the sphere, these spectra are functions of relative permeability (K), conductivity (σ), and characteristic body dimension (a). However, for time-constant spectra to be of benefit as a target classification tool, it is necessary that these spectra be cataloged for shapes of interest. We know from the literature cited, that it is possible to compute these modal parameters for arbitrary shapes. However, we have yet to develop programs for numerical modeling. Thus, our knowledge of the behavior of time-constant spectra is restricted to published relations for the values of the principal (longest) time constant appropriate for certain canonical shapes [5]. These relations do not include the effect of relative permeability and describe only the "late stage" of the TEM decay transient that is dominated by the term in (1) with the longest time constant.

3.1 Data Acquisition System

It is clear from modeling that resolution of higher order time constants of a TEM transient requires a fast TEM system with a large dynamic range. Zonge Engineering has developed the NanoTEM™ system [8], consisting of a battery-powered transmitter with a fast turnoff time (~1 μs into low inductance loops) together with a high-speed digital data acquisition system. The NanoTEM system simultaneously acquires up to 3 channels of data at a maximum sample rate of 800 kSample/s on each channel. A measure of bandwidth of a TEM decay transient is the inverse of the current turnoff time ($1/T_0$). If the transmitter is turning off the current in 10μs, for example, the resulting decay transient will have a frequency bandwidth on the order of 100 kHz. The NanoTEM system can generate and measure decay transients starting at delay times on the order of 1 μs out to several milliseconds. An equivalent broadband FEM system must sample the frequency spectrum over a range of $0.5 \leq f \leq 500$ kHz.

Figure 5: Data Acquisition System

The elements of the system are shown Figure 5. In the background is a 3-in steel ball (mill ball) inside transmitter and receiving coils. The system was used to measure decay transients from many of the smaller targets shown in Figure 6. To simulate realistic survey conditions, the antennas were mounted on a cart (not shown). The system normally acquires a stacked transient consisting of 31 samples on logarithmically spaced time intervals.

Figure 6: Assorted UXO Targets

3.2 UXO Characterization Experiments

With the data acquisition system previously described, we conducted experiments aimed at characterizing various pieces of UXO and other small objects (Figure 6) to determine their characteristic TEM transient response under controlled stimulation. For these experiments, objects are placed in a known source field. The resulting transients are reduced to obtain a measure of their magnetic polarizability.

3.2.1 Data Reduction For Magnetic Polarizability

From equation (2), the magnetic moment of the object is given by the relation $\vec{M} = \vec{\vec{M}} \cdot \vec{H}_0$, where $\vec{\vec{M}}$ is the magnetic polarizability dyadic. The use of a dyadic or tensor to describe the polarizability of a target provides for the likelihood that most UXO will polarize anisotropically. That is, in general, the magnetic moment induced in the target will not be parallel with the

primary field. The polarization dyadic is symmetric and is ***aspect*** dependent. Its properties are dependent upon a coordinate system that is fixed to the target. In the context of equation (2), therefore, the polarizability dyadic is a function of three aspect angles (e.g., heading, pitch, and roll) that the UXO-fixed coordinate system makes with the coordinate axes of the measurement system. The polarization dyadic is diagonal when expressed in its ***principal coordinate system***. Moreover, when there are symmetries in the target, the polarization dyadic will be invariant under coordinate rotation about the axis of symmetry. It should be clear, therefore, that the polarizabilty dyadic of a sphere is isotropic and proportional to the identity matrix.

In those cases where UXO exhibits a single axis of cylindrical symmetry (say, the z-axis in the *principal system*), the polarizability dyadic will take the form

$$\vec{M} = \begin{bmatrix} P_T(t) & 0 & 0 \\ 0 & P_T(t) & 0 \\ 0 & 0 & P_L(t) \end{bmatrix} = \frac{1}{H_0} \begin{bmatrix} m_T(t) & 0 & 0 \\ 0 & m_T(t) & 0 \\ 0 & 0 & m_L(t) \end{bmatrix} \tag{5}$$

The subscript T signifies polarization that occurs when the polarizing field is transverse to the axis of symmetry, while the subscript L signifies polarization that occurs when the incident field is parallel to the axis of symmetry. We can use equation (5) to determine polarizability dyadic of UXO by measuring the TEM transient when the primary field (H_0) is aligned parallel (L) to the axis of symmetry (measure $m_L(t)$) and then by measuring the transient when the primary field is aligned transverse (T) to the axis of symmetry (measure $m_T(t)$).

A dipole with moment $m(t)$, centered in a circular[2] coil (with N_r turns) having radius a and directed perpendicular to the plane of the coil, will generate a voltage given by

$$v(t) = -\frac{\mu_0 N_r}{2a}\frac{dm(t)}{dt} = \sum_{i=1}^{N} B_i e^{-\frac{t}{\tau_i}} \tag{6}$$

We use Prony's method to find the residues and time constants on the right side of equation (6). By integrating equation (6) with respect to time (t), we find a relation for the effective moment of the dipole

$$m(t) = \frac{2a}{\mu_0 N_r}\int_{\infty}^{t} v(t)dt = \frac{2a}{\mu_0 N_r}\sum_{i=1}^{N} \tau_i B_i e^{-\frac{t}{\tau_i}} \tag{7}$$

Combining equation (5) with (7) we obtain a relation for magnetic polarizability

$$P(t) = \frac{2a}{\mu_0 N_r H_0}\int_{\infty}^{t} v(t)dt = \frac{2a}{\mu_0 N_r H_0}\sum_{i=1}^{N} \tau_i B_i e^{-\frac{t}{\tau_i}} \tag{8}$$

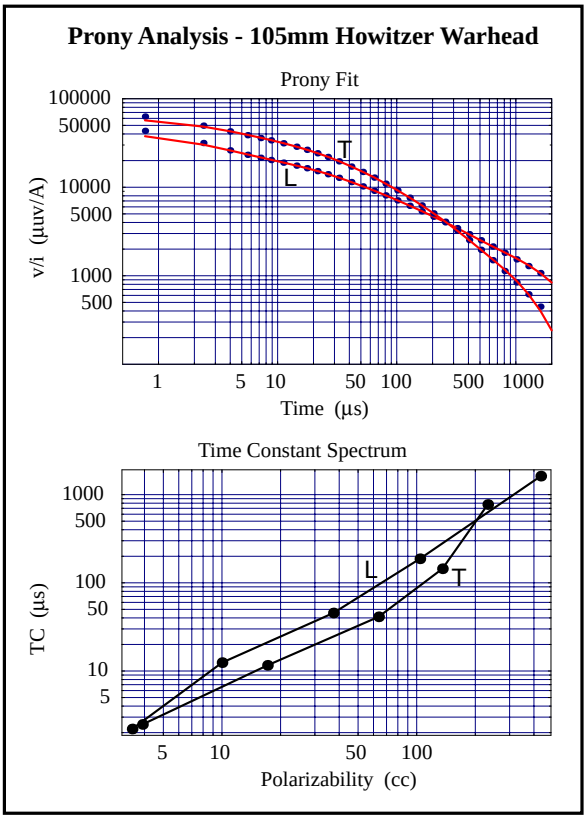

Figure 7: Representative experimental decay transients and their spectra

[2] In the analysis leading to the determination of normalization factors for computing moments and magnetic polarizability we have used the approximation that the voltage induced in a square coil of radius a may be approximated by the voltage that would be induced in a circular coil with the same cross sectional area.

3.2.2 Polarizability Characterization Experiments

Objects were placed in the field of either a small (0.5m x 0.5m) coil (Figure 5) or, for larger targets, in the field of the 5ft x 5ft Helmholtz coil (not shown). When the objects had an axis of symmetry, transients were measured in both longitudinal (L) and transverse (T) directions. Figure 7 illustrates a NanoTEM transient observed in the course of our characterization experiments. These data are normalized for instrument gain and transmitter current only. Signal levels have not been adjusted for either transmitter or the receiver geometry. The observed data together with its fit using Prony (*Prony Fit*) are above. The plot labeled *Time Constant Spectrum* indicates values for the time constants and residues. We have again plotted the discrete spectra as lines connecting points to facilitate identification of each spectrum. The magnetic polarizability value *P(0)* for each of the targets shown has been calculated using equation (8). Values of *P(0)* and the principal (longest) time constants for tested objects are tabulated in Table 1. Note that some targets have principal time constants that are as short as a few hundred microseconds. Thus, in order to resolve three or four of the higher order time constants, it is essential that the TEM system have a time bandwidth that ranges from microseconds to a few milliseconds (three decades).

Table 1: Polarizability and Principal Time Constants for Tested Objects

Target	Longitudinal Polarization		Transverse Polarization	
	P_l (cm^3)	τ_0 (μsec)	P_T (cm^3)	τ_0 (μsec)
20mm Projectile	64	781	16	580
2.25" Rocket Head	66	1097	86	1113
3 2.5" Steel Washers	67	754		
Spherical Handgrenade	93	356		
6 2.5" Steel Washers	110	884		
M12 Handgrenade	151	221	118	264
6"x7"x1/8" Al Plate	168	497		
3" Diameter Steel Mill Ball	1168	701	0	N/A
60mm Mortar Round	2407	923	708	456
75mm Artillery Round	3965	1455	2460	660
Anti-Tank Rocket	4407	850	1062	361
90mm Mortar Round	5664	1169	2177	674
105mm Artillery Round	10408	1622	8000	773
3.5" Steel Pipe	8897	974	5312	526

3.2.3 UXO Survey Simulation

We simulated surveys over buried targets using a cart-mounted antenna array (not shown) similar to that of an EM-61. Surveys were conducted in a "stop and go" mode wherein measurements were acquired at intervals of ½ m. We show here the results from a single profile of the vertical field component taken over a target consisting of a 1-ft length of 3.5" diameter steel pipe buried at a depth of 15" to its center. The pipe was buried so that its axis was vertical. The polarizability parameters that we measured have been tabulated in Table 1 (3.5-in Pipe). The behavior of the transient when polarized along its longitudinal (L) and transverse (T) axes is shown in Figure 8.

Six transients for the vertical component of the secondary fields are plotted in Figure 9. Each

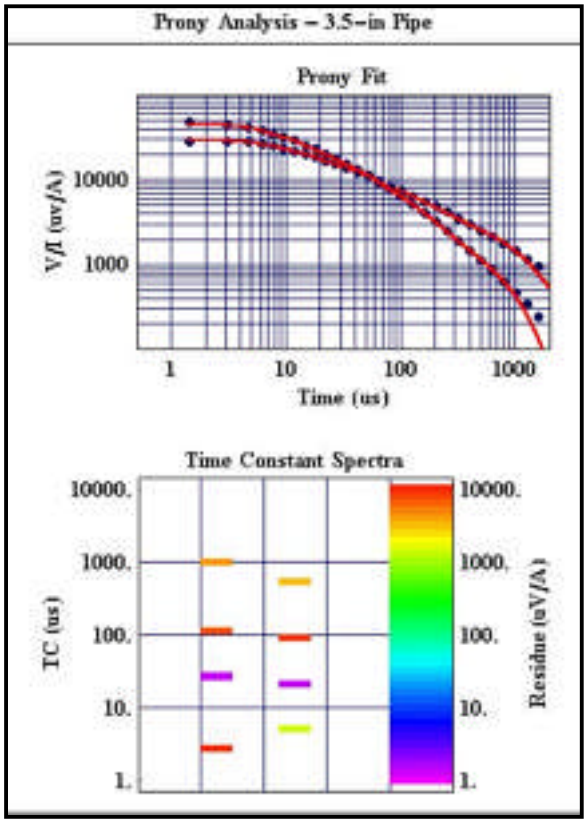

Figure 8: TEM transient - 3.5" Pipe

transient plot is annotated with its position (x) along the measurement profile. The target is located at x=2.5m. At early time (.001 to 0.01 ms), the transients drop sharply. This decay trend continues down to instrument noise levels for the 4 antenna positions (x=1.0, 1.5, 3.5, 4.0). In contrast, the 3 transients measured while the transmitter is at least partly over the target (i.e., x=2.0,2.5,3.0), exhibit decay that extends to the end of the measurement time (1.911 ms). Figure 10 is a composite plot of a simulated EM-61 profile (left), and the associated time-constant spectra. We have modulated the plot pixel of the spectra plot with a gray level to give an indication of the amplitude of the residue of the associated time constant. The longest time-constant is observed when the transmitter is centered directly over the target where the polarizing field H_0 is vertical and hence is parallel (Longitudinal) to the target's axis of symmetry. The transients measured ½ m on either side of the target exhibit moderately lower time constants. These transients were observed at a point where a side of the transmitter loop was located directly over the target. Here, the polarizing field is horizontal (Transverse) to the target axis. This behavior agrees with the polarizability characteristics for the 3.5" pipe (see Table 1). Note that the amplitude of the residue of the second time-constants are larger than those of the principal time constants, a behavior that renders permeable targets more detectable in the early time. The behavior is also consistent with time-constant spectra for a conducting permeable sphere (Figure 3) and suggests that the target has high relative magnetic permeability.

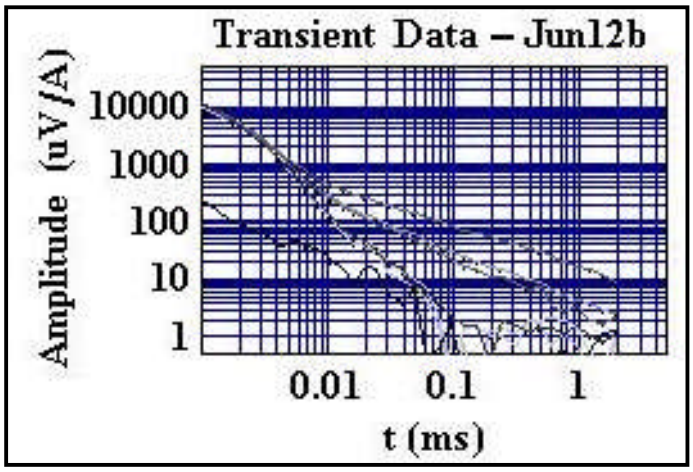

Figure 9: Vertical field TEM transients along survey profile

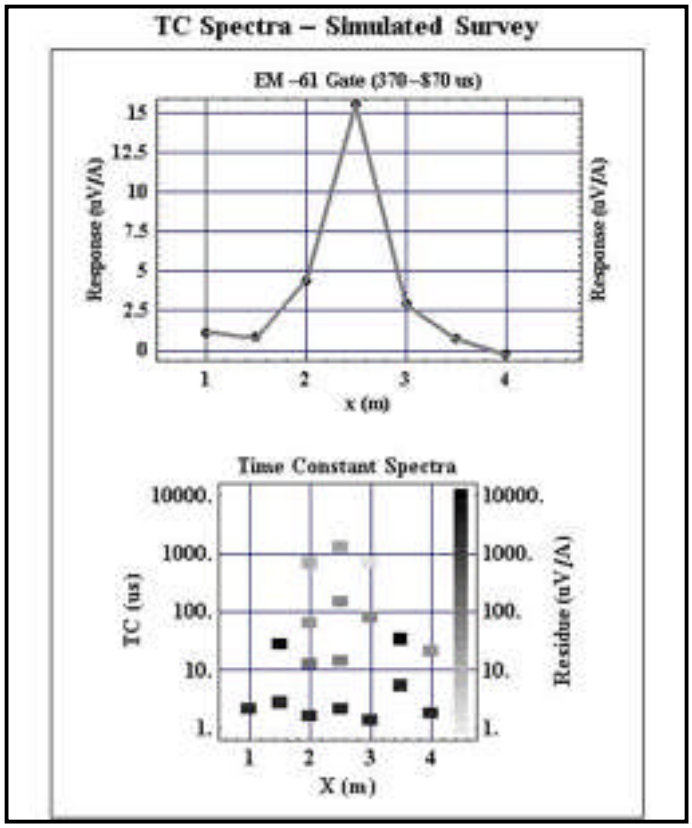

Figure 10: Time constant spectra. Test line (target at x=2.5m)

The characteristic TEM transients shown in Figure 8 were acquired using a large (i.e., 5ft x 5ft) Helmholtz transmitter coil. Using the results of the Prony decomposition together with equation (8), we are able to calculate a time-varying polarization tensor as shown in equation (5). Then, assuming that the

secondary field behaves like a point dipole in accordance with equation (2), we calculated the response of our antenna system over the pipe target for 2 cases: a) Horizontal orientation; b) vertical orientation. These results are shown as Figure 11. We haven't yet run experiments with the pipe target buried in a horizontal position. But the behavior of the spectra for the vertical pipe is similar to that observed in Figure 10. When the antenna array is directly over the vertical pipe, the pipe is being polarized along its longitudinal axis and therefore it exhibits a longer characteristic decay time. When the antenna is displaced ½ m to either side of the target, the primary field is mainly horizontal and therefore excites the transverse mode of decay and the field exhibits the characteristically shorter decay times for the transverse mode of polarization. If the target is horizontal (left side of Figure 11), the effect is just the opposite. We observe shorter decay times when directly over the target (transverse polarization mode), and longer decay times when off the target (longitudinal polarization mode). Because the data for this figure is noise free and has effectively infinite dynamic range, the time constants observed at distances of several transmitter loop diameters (where the primary field is vertical) behaves as it does when the directly over the target. As a practical matter however, the primary field is too small to generate a measurable secondary field. Therefore, in practice, we do not observe a TEM response at horizontal distances beyond a loop diameter.

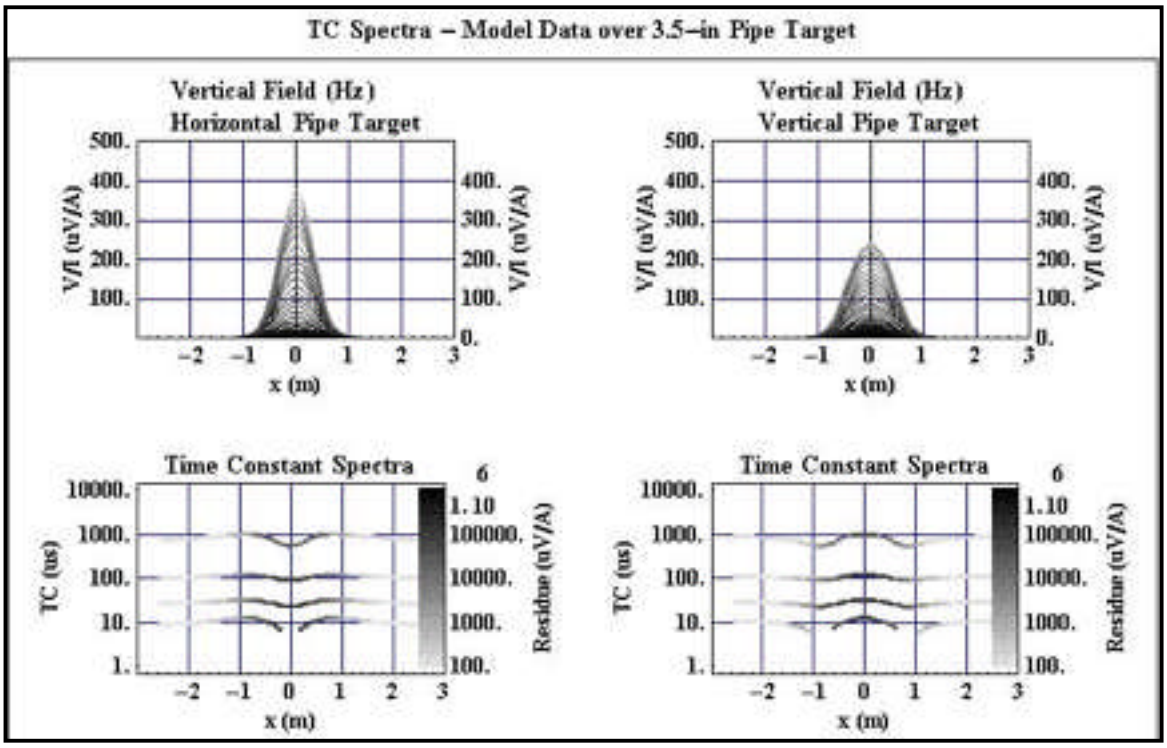

Figure 11: Time-constant spectra for a synthetic NanoTEM profile over a pipe model using a experimentally derived polarization tensor

Figure 11 demonstrates that a target with anisotropic polarizability generates a signature in the time constant plots that is easily recognized. The sphere, on the other hand, has an isotropic polarizability tensor. Consequently, the shape of the transient curve does not vary with position. In Figure 12 we have generated spectral plots using synthetic TEM data calculated over a conducting sphere. The left side of the figure is for the case of a conducting sphere with relative permeability K=1. The right side is for the case of a permeable sphere (K=500). Unlike the pipe model, the time constant spectra is constant regardless of position along the profile.

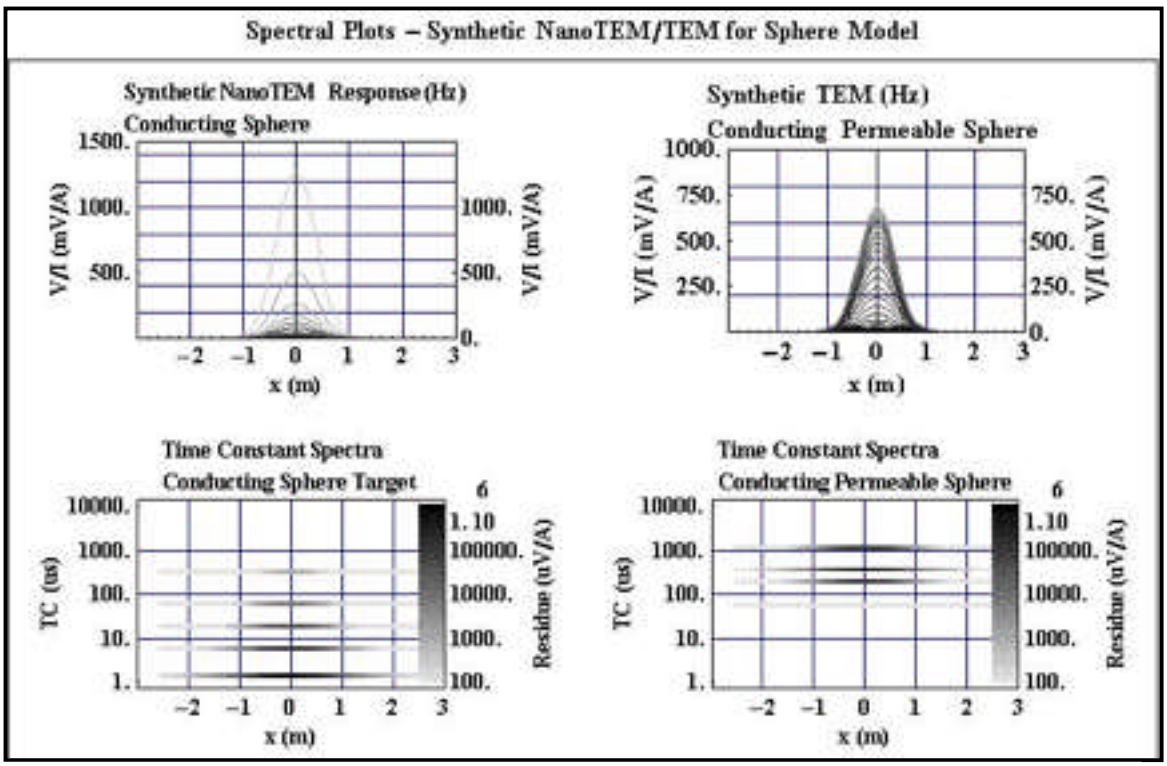

Figure 12: Time-constant spectra for a synthetic TEM profile over a sphere model. (Left -K=1; Right – K=500)

4.0 CONCLUSIONS

We have demonstrated that TEM decay transients from small targets such as UXO can be parameterized to provide useful target classification information. We use a dipole model and Prony decomposition to analyze TEM transients from UXO targets. These results (see Table 1) provide estimates of the magnetic polarizability dyadic. Theoretical and experimental time-constant spectra show that permeable targets exhibit residues that are larger for higher order time constants than those for the principal (longest) time constant. Our results emphasize the need for a fast TEM or equivalent broadband FEM system since small objects (e.g., hand grenades) have measurable high order time constants that may be less than 10 μs. Full characterization of the target including its position, polarizability dyadic in the principal coordinate system, and the aspect angles requires at least 8 independent transient field measurements made with different directions of field polarization. It is important, therefore, that vector components of the transient field be measured to provide the independent measurements necessary for solution of the problem. Our experimental system, similar in many respects to the EM-61, can simultaneously measure the full TEM transient of three field components. Actual identification of a target requires that the polarizability dyadic be compared with a library of dyadics for targets of interest. An effort to construct a comprehensive library of intrinsic target polarizability dyadics using experimental and numerical characterization is warranted.

5.0 REFERENCES

1. McNeill, J.D., and Miro Bosnar, *Application of Time Domain Electromagnetic Techniques to UXO Detection*. in *UXO Forum 1996*. 1996. Williamsburg, VA.
2. Geng, N., Baum, Carl E., and Carin, Lawrence, *On the Low-Frequency Natural Response of Conducting and Permeable Targets.* IEEE Trans. on Geosci. and Rem. Sensing, 1999. **37**(1): p. 347-359.
3. Baum, C.E. (editor), 1999, *Detection and Identification of Visually Obscured Targets*, Taylor & Francis, Philadelphia, PA.
4. Kaufman, A., *Frequency and Transient Responses of Electromagnetic Fields Created by Current in Confined Conductors.* Geophysics, 1978. **43**(5): p. 1002-1010.
5. Kaufman, A.A., *A Paradox in Geoelectromagnetism, and its Resolution, Demonstrating the Equivalence of Frequency and Transient Domain Methods.* Geoexploration, 1989. **25**: p. 287-317.
6. Wait, J.R., and Kenneth P. Spies, *Quasi-static Transient Response of a Conducting Permeable Sphere.* Geophysics, 1969. **34**(5): p. 789-792.
7. Van Blaricom, M.L., and Mittra, Raj, *A Technique for Extracting the Poles and Residues of a System Directly from Its Transient Response.* IEEE Trans. on Ant. & Prop., 1975. **AP-23**(6): p. 777-781.
8. Mauldin-Mayerle, C., Norman R. Carlson, and Kenneth L. Zonge. *Environmental Application of High Resolution TEM Methods*. in *The 4th Meeting on Environmental and Engineering Geophysics*. 1998. Barcelona, Spain: European Section, EEGS.